Preferential Outward Diffusion of Cu during Unconventional Galvanic Replacement Reactions between $HAuCl_4$ and Surface-Limited Cu Nanocrystals

Yonglin Liu* and Angela R. Hight Walker

Optical Technology Division, Physics Laboratory, National Institute of Standards and Technology, Gaithersburg, Maryland 20899-8443, United States

ABSTRACT Metal diffusion in nanoscale materials is of great interest, yet the detailed kinetic behavior of such diffusion remains elusive. We observe direction-controlled Cu diffusion during unconventional galvanic replacement reactions between surface-limited Cu nanocrystals (NCs) and $HAuCl_4$. Using presynthesized $Cu-Cu_{1.81}S$ hetero-oligomer and $Cu-Cu_2S$ heterodimer NCs as templates and reactants, the controlled addition of $HAuCl_4$ leads to the preferential outward diffusion of Cu, visualized by the formation of single-crystalline and straight, or polycrystalline and kinked, CuAu nanowires, respectively. The time-dependent growth of these nanowires enables determination of nanoscale diffusion coefficients of Cu during these processes, for the first time.

KEYWORDS: Cu diffusion · nanomaterials · unconventional galvanic replacement reaction · surface-limited Cu nanocrystals · diffusion coefficient

The diffusion of noble metals is of great importance and interest in the fields of electronics,[1−8] catalysis,[9] and biotechnology.[10] For instance, as a major interconnect material, the diffusion of copper (Cu) in conducting, dielectric, and diffusion barrier thin films has a direct effect on the performance of submicrometer integrated circuits.[2−8] It was not until recently[11−13] that the noble metal diffusion in nanomaterials started to be explored and occasionally applied to produce nanocrystals (NCs) with novel morphologies that are otherwise difficult to produce. In contrast to the well-studied metal diffusion in bulk,[14−16] on thin films,[17,18] and on the surface of substrates,[19−22] the diffusion behavior (kinetic, diffusion coefficient, *etc.*) of noble metals in nanostructured materials remains elusive, despite the impending need when the metal NCs are integrated[23−26] or assembled into building blocks[27−37] for future devices. One of the major obstacles is the lack of reliable protocols for such diffusion measurements in nanoscale materials. In the typical diffusion studies of bulk materials, metal films are first deposited on a substrate surface and heated to a high temperature. The resulting metal concentration profile on the substrate leads to diffusion distances and diffusion coefficients. It remains a technical challenge to apply this method directly to the study of nanoscale materials.

Noble metal diffusion in nanomaterials has been detected in several cases, including Au diffusion in semiconductor NCs,[11−13] the diffusion of Cu atoms into presynthesized Au NCs to form Cu−Au alloy NCs,[38] and metal pair diffusion in nanoscale galvanic replacement reactions (GRRs).[39−48] The diffusion and coalescence of Au−Pd and Au−Cu bimetallic nanoparticles were also reported by Sacher[49] and Howe[50] and their co-workers, respectively. Recently, Alivisatos, Dahmen, and co-workers observed real-time diffusion of Au NCs in an aqueous thin film using transmission electron microscopy (TEM).[51] The diffusion of Cu NCs was also observed on the surface of amorphous alumina[19] and Pd(110).[52] The self-diffusion of Cu within polycrystalline nanomaterials was investigated using radioisotope techniques by Gleither and co-workers.[53] Among these observations, nanoscale GRRs provide a powerful route to produce bimetallic NCs with hollow interiors. By taking advantage of the nanoscale "Kirkendall effect",[54] this protocol demonstrates that the different diffusion rates of two metal species across the interface can cause the formation of voids. For instance, Xia and co-workers reported the production of hollow bimetallic NCs with various morphologies such as nanocages, nanoboxes, nanorings, and nanoframes, using Ag NCs as templates and starting

* Address correspondence to yonglinliu06@gmail.com.

Received for review February 11, 2011 and accepted August 25, 2011.

Published online August 25, 2011
10.1021/nn200565y

materials.[48,55−59] During these conventional GRRs, the rather fast reaction times (in a few seconds to minutes) combined with the comparable diffusion rates of two metal species usually leads to the formation of products with similar morphologies to the starting NCs. The absence of distinctly directional nanostructures makes it impossible to identify the metal diffusion distance required for the calculation of diffusion coefficients. Additionally, during Au diffusion in semiconductor NCs,[11−13] it has been shown that Au atoms first diffuse in all directions, and then these atoms come together to form a single Au NC within or on the surface of each semiconductor NC due to Ostwald ripening. Recently, Alivisatos and co-workers described cadmium (Cd) diffusion during the NC sulfidation process, where time-dependent metal core evolution leads to the measurement of Cd diffusion coefficients.[60] Diffusion coefficients in nanocrystalline materials can be orders of magnitude different from their bulk counterparts.[53,60] A simple protocol of measuring diffusion coefficients in NCs is of great importance and is the goal of this work.

We recently reported a facile and efficient protocol to produce Cu−$Cu_{1.81}S$ hetero-oligomer and Cu−Cu_2S heterodimer NCs.[61] The Cu portions among these hetero-oligomers and heterodimers show limited open surfaces due to the later growth of copper sulfide portions.[61] In the present study, we demonstrate that Cu diffusion, during the nanoscale GRR with Au^{3+}, can take place in both time- and direction-controlled manners, when the reaction is constrained to within a few tens of nanometers of the Cu NC surface. Using presynthesized Cu−$Cu_{1.81}S$ hetero-oligomer and Cu−Cu_2S heterodimer NCs as templates and reactants, the controlled addition of $HAuCl_4$ leads to the preferential outward diffusion of Cu, as evidenced by the formation of straight, single-crystalline or kinked, polycrystalline CuAu alloy nanowires, respectively. The directional structures of the as-prepared CuAu nanowires elucidate the outward diffusion pathway of Cu, visualized by alloying Cu with newly produced Au. The time-dependent growth of these nanowires enables determination of the diffusion coefficients of Cu during these processes for the first time.

RESULTS AND DISCUSSION

Three different nanostructures, namely, Cu NCs, Cu−$Cu_{1.81}S$ hetero-oligomers, and Cu−Cu_2S heterodimers, are produced from the wet chemical reactions following our previous reported procedures.[61] These three nanostructures are used as starting NCs for GRRs with $HAuCl_4$. In particular, the Cu diffusion products were obtained after the predetermined amount of $HAuCl_4$ solutions (in diethylene glycol) were directly added into the presynthesized hetero-oligomer or heterodimer solutions in the absence of any purification process, and the temperature of the reaction solution was maintained at 180 °C. The diffusion behavior of Cu in these three systems is studied through characterization of the resulting nanostructures following GRRs.

GRRs of Cu NCs. Although the surface-limited redox replacement reactions between bulk Cu substrates[62] or Cu films[63] and metal ions were previously studied, GRRs using Cu NCs as sacrifice templates have yet to be reported, possibly due to the difficulty of Cu NCs' synthesis. The GRR of colloidal Cu NCs with $HAuCl_4$ has thus been investigated. Cu NCs were produced following our recently reported procedure,[61] and the as-prepared Cu NCs show a large size distribution with an average of 33.0 ± 18.3 nm (Figure 1). High-resolution TEM (HR-TEM) image and the inserted image of calculated fast Fourier transform (FFT) of the selected areas indicate the polycrystalline nature of these NCs (Figure 1). Following the GRR between Cu NCs and $HAuCl_4$ in diphenyl ether at 180 °C, the derived products are shown in Figure 2. Two types of nanostructures are observed. Larger NCs, with an average size of 39.4 ± 7.8 nm in diameter, have hollow interiors and, as seen in the HR-TEM image in Figure 2b, are characterized by cage-type structures. HR-TEM images also show multidirection lattice planes, confirming the polycrystallinity of these resulting nanocages and providing a wall thickness from 5 to 15 nm. On the other hand, smaller NCs, averaging 15.1 ± 4.1 nm in diameter, show homogeneous TEM contrast throughout each nanoparticle, indicating solid NCs are produced. Energy dispersive X-ray (EDX) taken from multiple nanoparticles demonstrates that both the larger nanocages and the smaller, solid NCs were composed of an Au−Cu alloy, with the approximate Au to Cu atomic ratio of 1:1 (Figure S1 in the Supporting Information). The size-dependence Kirkendall effect, as we observed here, has been previously reported during the oxidation of nickel NCs.[64] It has been reported that the GRR between Ag NCs and $HAuCl_4$ results in Au or Au−Ag alloy shells only when the starting Ag NCs have dimensions larger than 20 nm.[58,65] The GRR reaction starting with smaller Ag NCs (<20 nm) leads to the formation of solid Au−Ag alloy NCs.[42] Likewise, our above experimental observations show a similar size-dependent reactivity of Cu NCs, and there appears to be a critical size on the order of 20 nm for Cu NCs during their GRRs with $HAuCl_4$. When Cu NCs are smaller than 20 nm, solid Au−Cu alloy NCs are formed (Figure 2c). Above ~20 nm, Au−Cu alloy nanocages are produced (Figure 2b). This phenomenon can be explained thermodynamically, since below the size of 20 nm, the nanoparticles are too small to make stable hollow structures.[66] Li and co-workers recently demonstrated that monodisperse, intermetallic CuAu NCs below 10 nm can be produced by diffusing newly produced Cu atoms into presynthesized Au NCs.[38]

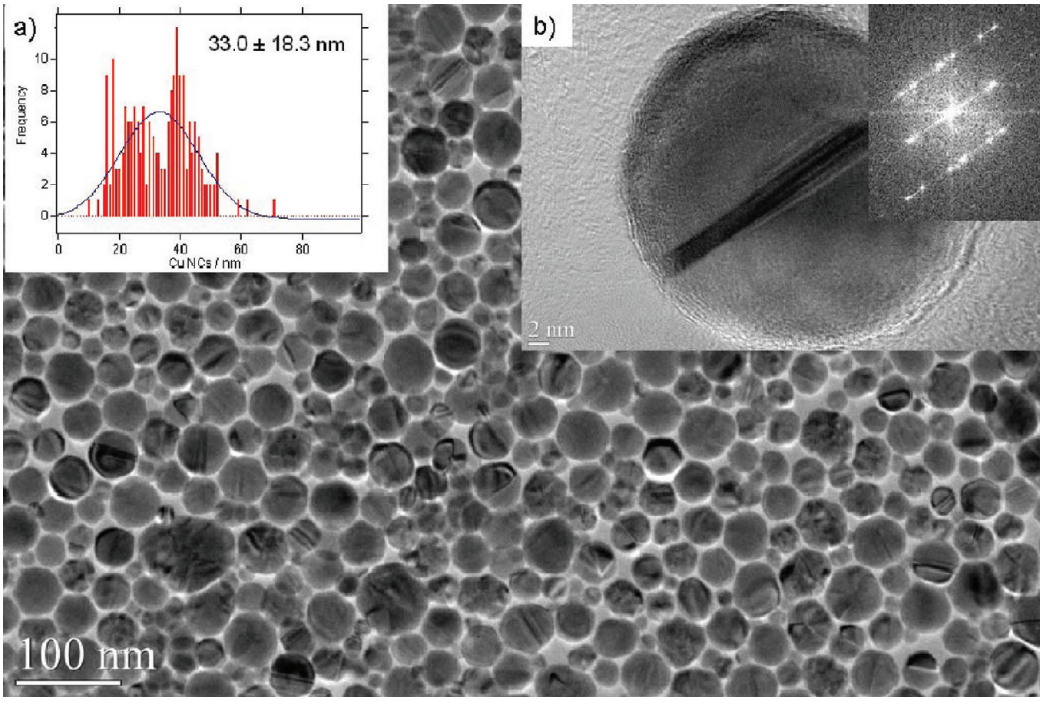

Figure 1. TEM images of as-prepared Cu NCs. (a) Histogram of the Cu NCs by counting 200 nanoparticles. (b) HR-TEM image of one typical Cu NC and the calculated FFT of the selected area showing the polycrystalline nature of the NCs.

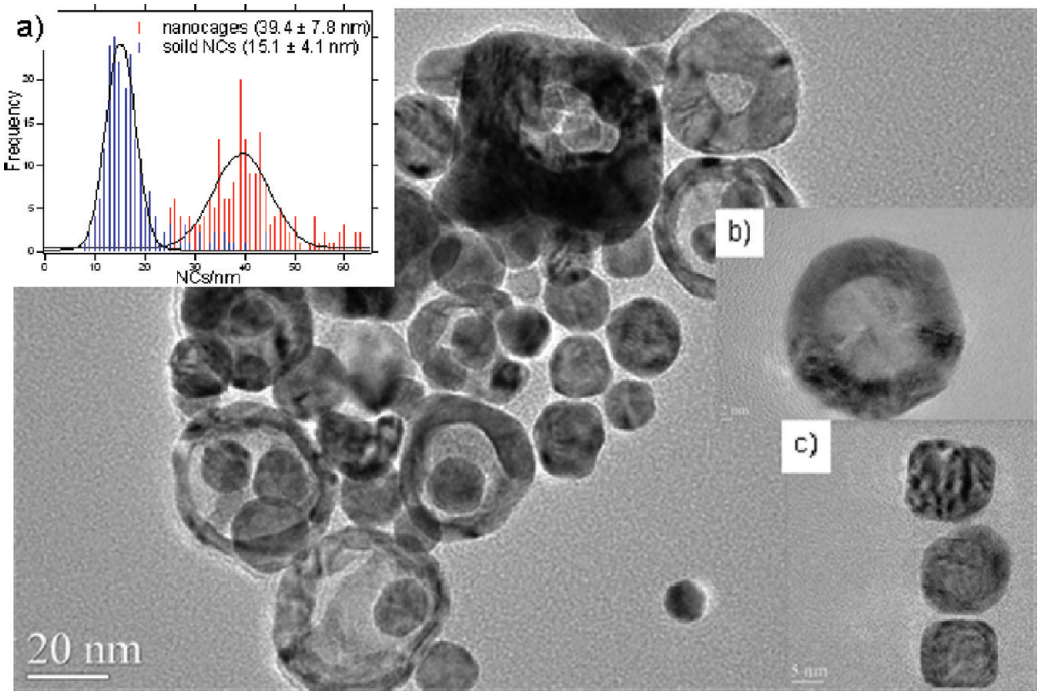

Figure 2. TEM images of Au−Cu NCs obtained after the addition of $HAuCl_4$ into the solution of Cu NCs. Insets (a, b, and c) showing histograms of as-prepared NCs, HR-TEM images of one typical nanocage, and three solid NCs, respectively.

We demonstrate here that the diffusion of Au atoms into Cu NCs (<∼20 nm) can also produce alloy CuAu bimetallic NCs.

GRRs of Cu−$Cu_{1.81}S$ Hetero-oligomers. The hetero-oligomers of Cu−$Cu_{1.81}S$ were produced following our previously reported protocol.[61] As shown in Figure 3a and c, the Cu and $Cu_{1.81}S$ domains can be easily differentiated by the TEM contrast brightness. In each oligomer, the single-crystalline Cu domain (the dark center) is covered by multiple $Cu_{1.81}S$ nanoparticles (the lighter branch area) with periodic open Cu surfaces of a few nanometers.[61] It has been previously reported

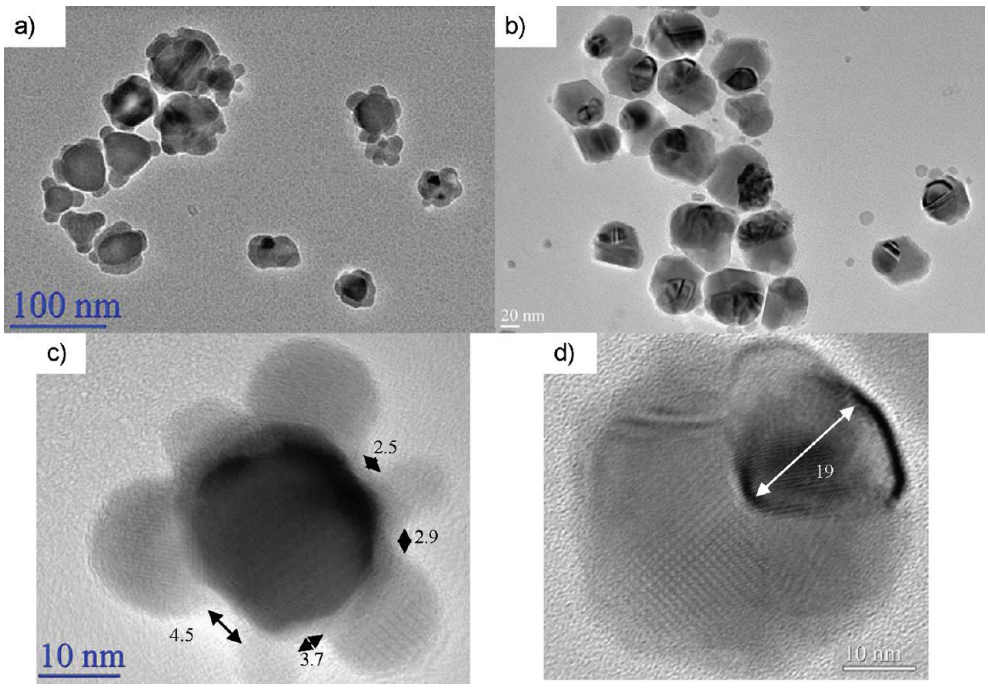

Figure 3. TEM images of (a) Cu−$Cu_{1.81}S$ hetero-oligomers and (b) Cu−Cu_2S heterodimers. HR-TEM images of one single (c) Cu−$Cu_{1.81}S$ hetero-oligomer and (d) Cu−Cu_2S heterodimer, showing limited open surfaces of metal Cu domains.

that the GRR of metal NCs a few nanometers in size results in nanostructures different from their larger counterparts.[42,67] Thus, the GRR of Cu domains in hetero-oligomers with $HAuCl_4$ under such limited reactive surfaces is expected to show different reactivity from that of unmodified Cu NCs as described above. After the dropwise addition of a $HAuCl_4$ solution (95 mg in 3 mL of diethylene glycol (DEG)) into the oligomer solutions, the as-prepared NCs are shown in Figure 4. At 7 min, it appears that nanowires start to form on the open surfaces of Cu domains (Figure 4a). These nanowires continue to grow at 15 min (Figure 4b) and 30 min (Figure 4c), until approximately 60 min, when they reach their maximum length (Figure 4d and e). EDX analysis, elemental mapping analysis, and scanning transmission electron microscopy (STEM), in conjunction with EDX line scan profiling along the diameter of a typical nanowire, reveal that these nanowires are a homogeneous alloy of Cu and Au with an approximate atomic ratio of 1.3:1 (Figure S2 in the Supporting Information). This observation represents a significant difference from conventional nanoscale GRRs, where hollow NCs with similar morphologies to those of sacrificed metal NCs were usually produced.[43−48] HR-TEM image of one typical nanowire (Figure 4f) shows that each nanowire is composed of periodic arrowhead-shaped single-crystalline units. These single-crystal units have an average side length of 12 nm and are epitaxially attached to one another mainly in the direction of [111] lattice fringe, leading to the formation of a single-crystal nanowire (Figure 4f). Some of these arrowhead-shaped units can also grow in the direction of [200] lattice fringe, forming branched nanowires (Figure 4b, c, and d, marked by stars and arrows). This phenomenon can likely be explained thermodynamically, since for noble metal crystals such as Au and Cu the surface energy relationship of three low-index crystallographic planes is γ [111] < γ [200] < γ [110].[68] Even though the detailed formation mechanism remains elusive and a complete study is under way, the production of single-crystalline nanowires composed of periodic arrowhead-shaped units is likely due to a heteroepitaxial growth mechanism. The measured *d* spacing analysis on the basis of the HR-TEM image shown in Figure 4f indicates that the CuAu alloy nanowire epitaxially attaches to the [111] plane of the Cu core through its [111] plane. The lattice mismatch along this direction can be calculated as [(0.207 − 0.200)/0.207 × 100%] = 3.4%. Such a small mismatch leads to a smooth epitaxial growth of face-centered cubic (fcc) CuAu alloy on fcc Cu without any obvious dislocation. As shown in Figure 4f, these single-crystalline and arrowhead-shaped units have an average side length of 12 nm and are epitaxially attached to one another mainly in the direction of [111] lattice fringe, leading to the formation of a single-crystal nanowire. These observations suggest that the epitaxial growth mechanism can be applied to explain the formation of the fcc crystalline structures of CuAu nanowires. It appears that the growth process is under thermodynamic control, where the resulting nanowires adapt to the most energentic stable structures. To approximate the most stable product, the formation of single-crystalline nanowires can be considered in

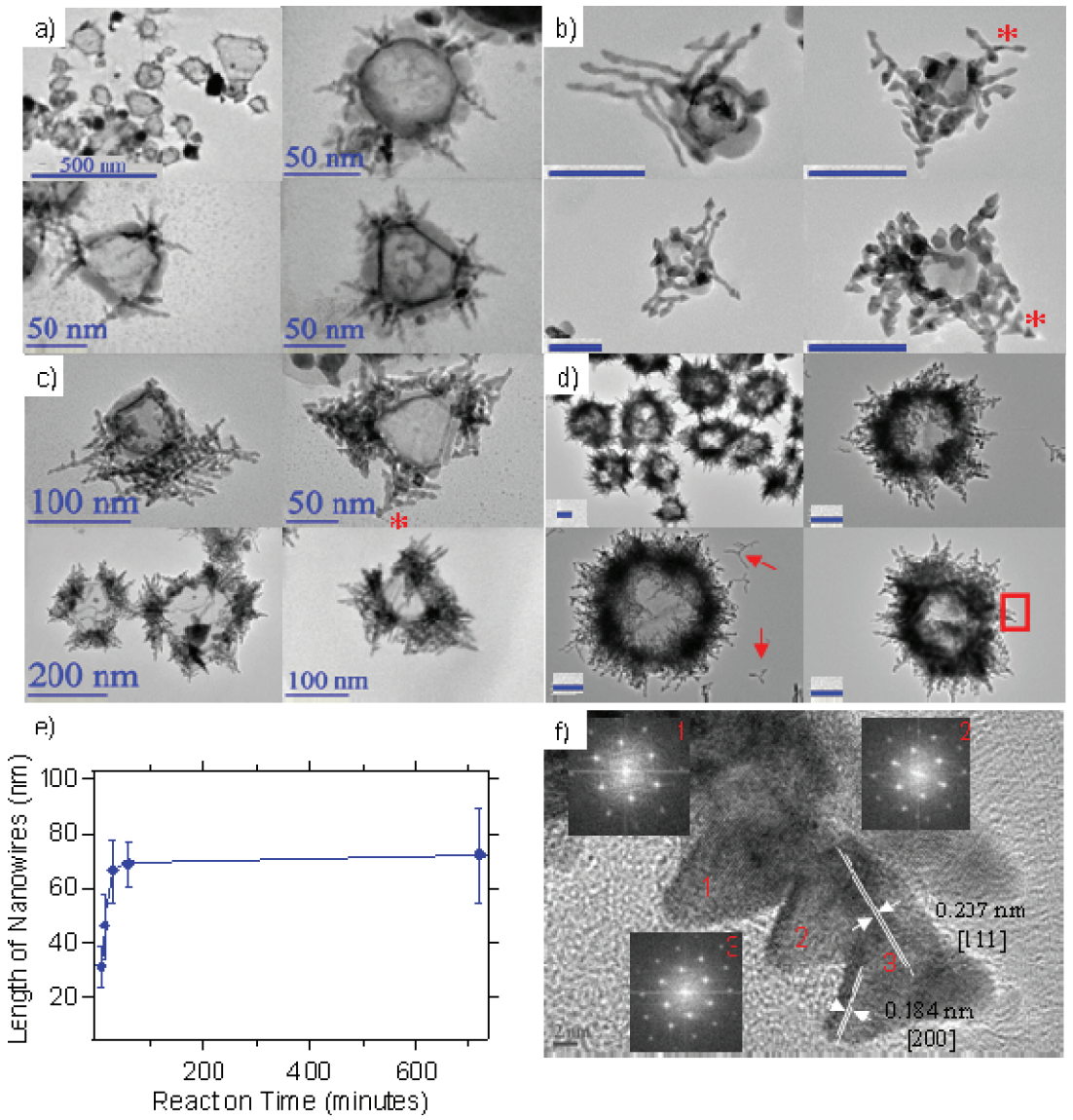

Figure 4. Outward diffusion of Cu is visualized as it is alloying with Au, shown as CuAu alloy nanowires sticking to the open surface of Cu domain in hetero-oligomers. TEM images of as-prepared nanowires observed at (a) 7 min, (b) 15 min, (c) 30 min, and (d) 60 min after the controlled addition of $HAuCl_4$ into the $Cu-Cu_{1.81}S$ hetero-oligomer solutions. (e) Plot of length of nanowires *versus* time showing the time-dependent growth of nanowires. (f) HR-TEM image of a selected area of one hetero-oligomer (marked as a red square in d). FFT images of selected areas showing single-crystalline structure across the whole nanowire. Stars mark branched nanowires, where NCs grow in the direction of [200] lattice fringe. Arrows mark isolated branched nanowires. All unlabeled scale bars represent 50 nm.

the context of Wulffs theorem,[69] which attempts to minimize the total interfacial free energy of the nanosystem. Since for noble metal crystals such as Au and Cu the surface energy relationship of three low-index crystallographic planes is γ [111] < γ [200] < γ [110], the resulting nanowires are composed of periodic arrowhead-shaped units, enclosed mostly by [111] facets. Thermodynamically, the formation of nanowires consisting of arrowhead-shaped units maximizes the expression of [111] facets and minimizes the total surface energy. Additional studies are underway to understand the factors determing the size of the arrowhead-shaped units, which likely include metal surface self-diffusion distance. For instance, gold (Au) has a much larger average surface self-diffusion distance (3−12 nm)[70] than copper (Cu), which might explain the average size of 12 nm of the arrowhead-shaped units.

It appears that the diffusion process of Cu atoms initiates at the open surfaces of Cu domains of hetero-oligomers, and it further occurs through the newly formed CuAu alloy nanowires (Figure 4). When Cu metal domains are subjected to GRR, Au^{3+} cations are reduced to Au atoms, which further form a CuAu alloy with Cu atoms (eq 1) on the limited, open Cu surfaces of the oligomers. Cu atoms from within the Cu domains then diffuse through the newly formed CuAu alloy interface of the nanowires to react with Au^{3+} to produce more CuAu alloy. The process repeats,

resulting in the formation of CuAu nanowires on the open Cu surface. At the CuAu alloy interface of the nanowires, the diffusion rate of atomic Cu appears to be much faster than that of Au^{3+}, which results in a net directional flow of matter outward. The alloying of Cu and Au takes place on a much faster time scale than the diffusion;[71] thus the growth of CuAu nanowires elucidates the outward diffusion of Cu. The instantaneous alloying of Cu atoms after diffusion with the newly formed Au makes it a unique way to visualize Cu diffusion. Each single-crystalline nanowire shows the directional pathway of Cu diffusion, representing a significant difference from the previously reported nanoscale metal diffusions.[11−13]

$$Cu + Au^{3+} \rightarrow Cu^{2+} + Au(alloy) \quad (1)$$

The outward diffusion of Cu can also be elucidated by the formation of voids within the Cu domains. For those oligomers with small sizes (tens of nanometers), the outward diffusion of Cu is comparable with its self-diffusion within the Cu domain, which results in single voids, indicated by homogenously light TEM contrast across the remaining Cu cores (Figure 4a). But for larger oligomers (greater than 100 nm), the formation of multiple voids (Figure S3a in the Supporting Information) or unevenly distributed metals in Cu domains (Figure S3b, c, and d in the Supporting Information) is likely due to the fact that self-diffusion is not fast enough to cause the voids to combine into a single void.

Ostwald ripening, a phenomenon of the growth of larger crystals from smaller ones due to the surface energy difference, has been previously observed during metal diffusion in semiconductor NCs.[11−13] The Ostwald ripening observed during those processes showed multiple-directional diffusion of metals in semiconductor NCs. Consequently, they usually lead to the formation of polycrystalline metal NCs. We propose that Ostwald ripening is not involved in the diffusion process described here for the hetero-oligomers, as each nanowire of CuAu alloy is a single crystal (Figure 4f).

This preferential outward diffusion of Cu over the inward diffusion of Au^{3+} depends critically on the manner of the addition of $HAuCl_4$. Slow and controlled addition of 95 mg of $HAuCl_4$ results in diffusion-controlled products (Figure 4). However, the instantaneous addition of 95 mg of $HAuCl_4$ into the hetero-oligomer solution leads to the formation of solid-core hybrid NCs (Figure S4 in the Supporting Information). Under this condition, the concentration of Au^{3+} around each hetero-oligomer immediately increases. As a result, the preferential inward diffusion of Au^{3+} over the outward one of Cu gives rise to solid-core CuAu (alloy)-copper sulfide hybrid NCs. Similar phenomena of the favored inward diffusion of Au were also observed during the GRRs of Au^{3+} with ultrathin Pd nanowires,[67] small Ag spherical NCs (<11 nm),[42,72] or small Cu NCs (<20 nm) (Figure 2 and Figure S1 in the Supporting Information).

TABLE 1. Diffusion Coefficients of Cu in Single-Crystalline CuAu and Polycrystalline CuAu NCs Determined in the Present Work,[a] Compared with Previously Reported Data in Polycrystalline Cu[b], and in Amorphous Alumina[c]

	diffusion coefficient of Cu (D, m^2/s)
in single-crystalline CuAu[a]	$(5.88 \pm 0.37) \times 10^{-19}$
in polycrystalline CuAu[a]	$(7.01 \pm 0.42) \times 10^{-19}$ to $(1.26 \pm 0.02) \times 10^{-16}$
in polycrystalline Cu[b]	2.11×10^{-16}
in amorphous alumina[c]	5×10^{-20}

[a] At 180 °C. [b] At 180 °C and determined by extrapolation to low temperature of diffusion data in previous studies.[53] [c] At 200 °C.[19]

The visualization of the Cu diffusion pathway through the formation of CuAu nanowires and their time-dependent growth allows us to investigate the kinetic behavior of this metal diffusion process. An estimate for the typical diffusion distance (X) with time (t) and diffusion coefficient (D) is given by eq 2.

$$X^2 = 4Dt \quad (2)$$

As shown in Figure 4e, at any given time, the diffusion distance was determined by measuring and averaging the lengths of ~200 CuAu nanowires from ~50 different nanostructures. The average diffusion coefficient of Cu was then calculated using three different times. The average diffusion coefficient of Cu within the hetero-oligomers is calculated as $(5.88 \pm 0.37) \times 10^{-19}$ m^2/s (Table 1). This work represents the first determination of Cu diffusion coefficient in single-crystalline CuAu alloy NCs. This measurement is in good agreement with the previously reported diffusion coefficient of Cu in small Au nanoparticles (3 nm)[73,74] at 1.1×10^{-19} m^2/s, and the interdiffusion coefficient of Ag and Au estimated as 1.0×10^{-19} m^2/s during the GRR between Ag nanoparticles and $HAuCl_4$.[75] However, this rate is approximately 1−2 orders of magnitude slower than the self-diffusion of Cu in polycrystalline nanomaterials as determined by the radioisotope method[53] and about 1 order of magnitude faster than that observed in amorphous alumina[19] (Table 1). Our result is reasonably consistent with these previous reports, since bulk phase Cu diffusion in polycrystalline materials can be up to 3 orders of magnitude faster than that in single crystals.[53]

GRRs of Cu−Cu_2S Heterodimers. Quite different from the hetero-oligomers, Cu−Cu_2S heterodimers have larger open surfaces (up to 20 nm) of Cu domains (Figure 3b and d). The Cu domains of these heterodimers likely undergo conventional GRRs to form hollow interior NCs. For instance, after the dropwise addition of 13 mg of $HAuCl_4$ into the dimer solutions, the TEM images of as-prepared NCs are shown in Figure S5 of the Supporting Information. The TEM images of NCs

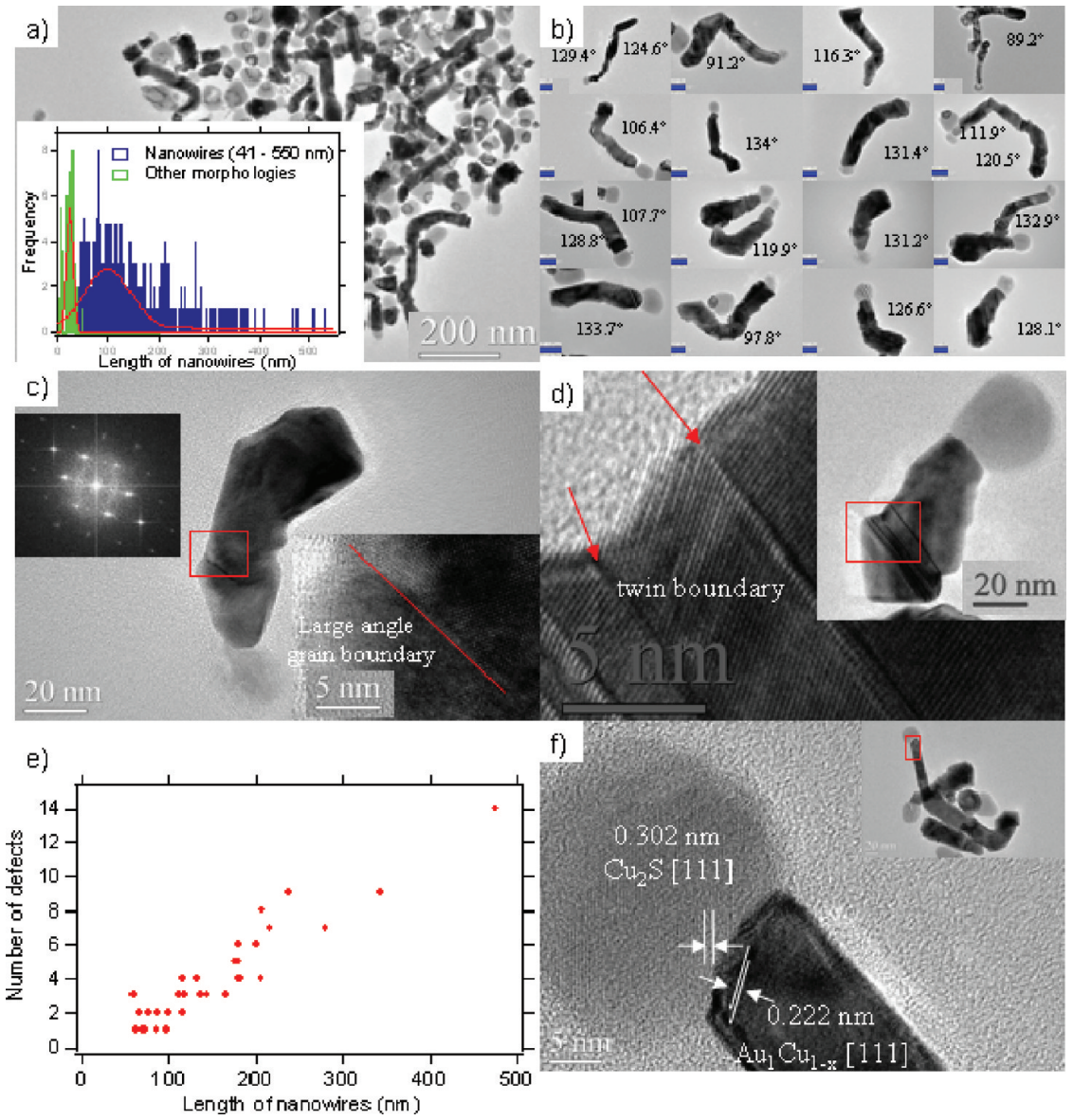

Figure 5. (a) TEM images and the histogram of as-prepared kinked nanowires along with NCs with other morphologies obtained 10 min after the controlled addition of $HAuCl_4$ into the Cu−Cu_2S heterodimer solutions. (b) TEM images of typical nanowires showing different angles. TEM and HR-TEM images of nanowires showing large (c) angle grain boundary or (d) twin boundary. (e) Plot of the number of defects *versus* the length of nanowires. (f) HR-TEM image of a selected area of one nanowire (marked as a red square in the inset image). All unlabeled scale bars represent 20 nm.

obtained after the instantaneous addition of 100 mg of $HAuCl_4$ into the dimer solutions are also shown in Figure S6 of the Supporting Information. It is unambiguous that for both cases hybrid NCs including hollow interiors of metal domains are formed. Notice that small amounts of NCs showing a solid core in the Cu domains are also observed after the instantaneous addition of 100 mg of $HAuCl_4$ into the dimer solutions, likely due to the mechanism similar to that of hetero-oligomers (Figure S4 in the Supporting Information). The resulting NCs with hollow interiors of Cu domains are due to the competitive rate between outward diffusion of Cu and inward diffusion of Au, leading to the formation of CuAu alloy nanocages of metal domains, similar to most of the conventional nanoscale GRRs.[39−48]

Nevertheless, the products showing preferential Cu outward diffusion were obtained after a 10 min reaction when 95 mg of $HAuCl_4$ in 3 mL of DEG was added slowly and dropwise into the heterodimer solution. As shown in Figure 5a, the as-prepared NCs are featured with kinked nanowires (~60% of the products) along with hybrid hollow NCs (~40% of the products). Most of the nanowires show bending angles of 90−130° (Figure 5b), comparable to the angle (109.5°) between two sets of [111] planes of fcc metals.[76] The elemental mapping analysis of a typical nanowire (Figure S7a, b, and c in the Supporting Information) and the EDX

investigation of multiple points along the nanowires demonstrate that each nanowire is composed of a homogeneous alloy of Cu and Au with an approximate atomic ratio of 1:1 (Figure S7d in the Supporting Information). The Cu_2S domains in the starting heterodimers remain intact during this diffusion process, shown in TEM as gray-colored, lower contrast sections connecting with one end of each nanowire (Figure 5b and Figure S7 in the Supporting Information). The HR-TEM image of the intersection between the metal nanowire and the Cu_2S nanoparticle further confirms that the Cu_2S domains remain single crystals (Figure 5f).

Our observations show that the diffusion process of Cu atoms initiates at the open surfaces of the Cu domains within the heterodimers, and it continues through the newly formed CuAu alloy nanowires (Figure 5). Interestingly, on the basis of the structural comparison between the starting heterodimers (Figure 3b and d) and the resulting nanowires (Figure 5b), the Cu atoms appear to diffuse in the opposite direction of Cu_2S domains. This phenomenon is likely due to the spatial steric hindrance effect. In the previous report of metal diffusion in semiconductor NCs,[11,12] a substitution-interstitial mechanism was proposed, where metal atoms substitute the interstitial sites of semiconductors and diffuse through the semiconductor layers. It was found that the migration of metal atoms usually distorts the atomic lattice of semiconductors, resulting in different crystallinity or amorphous structures. On the basis of our observations, the substitution-interstitial mechanism is unlikely taking place in the present process. The resulting nanowire structures and intact single-crystalline Cu_2S domains unambiguously elucidate the direct diffusion mechanism of Cu through these kinked nanowires in the absence of the involvement of Cu_2S. Similar to the case of hetero-oligomers, a heteroepitaxial growth mechanism can be proposed for the formation of polycrystalline and kinked nanowires for heterodimers, even though, at present, we are unable to observe the growth interfaces among the nanowires due to the complexity of the polycrystal of the Cu portions.

HR-TEM images (Figure 5) reveal that multiple kinds of defects exist along these kinked nanowires, in contrast to the single-crystalline diffusion products from hetero-oligomers (Figure 4). Figure 5c shows a typical nanowire with one large angle grain boundary, while the inset image of FFT on other locations of the wire shows single-crystallinity otherwise. In Figure 5d, TEM and HR-TEM images of one nanowire display several twin boundaries, where the different lattice orientation between two successive segments leads to the formation of a pattern of alternating contrast stripes. Additional crystal defects such as multiple twin boundaries and stacking faults are also found (Figure S8 in the Supporting Information). It is noted that the crystal defects in these nanowires can occur during the beginning (Figure S8a in the Supporting Information), the middle (Figure 5c and Figure S8b in the Supporting Information), or the end of the formation (Figure 5d). This observation is significantly different from kinked Au nanowires produced by mechanical disturbance, where the defects occur only *after* the kinked location.[76] It further confirms that these nanowires are produced by a diffusion-controlled mechanism, not by mechanical stirring.

Similar to the case of hetero-oligomers, each kinked nanowire shows the direct diffusion path of Cu; thus Cu diffusion coefficients can be estimated by using eq 2 for each single nanowire. The large range of nanowire lengths (41−550 nm) leads to a large distribution of Cu diffusion coefficients ($(7.01 \pm 0.42) \times 10^{-19}$ to $(1.26 \pm 0.02) \times 10^{-16}$ m^2/s) (Table 1). Notice that all of these diffusion coefficients are faster than that determined from the hetero-oligomers ($(5.88 \pm 0.37) \times 10^{-19}$ m^2/s). The observed Cu diffusion coefficient in polycrystalline nanowires ($(1.26 \pm 0.02) \times 10^{-16}$ m^2/s) is in better agreement with the previously reported data of polycrystalline Cu (Table 1),[53] indicating similar Cu diffusion behavior in polycrystalline nanomaterials. The different diffusion behavior of Cu through the resulting nanowires for these heterodimers from that for hetero-oligomers is likely due to the multiple-defect crystalline nature of the Cu domains of heterodimers.[61] It can be further confirmed by the defective crystal of the observed kinked nanowires. The crystal defects such as grain boundaries or dislocations can introduce fast diffusion pathways for metal atoms.[15−17,53,77]

We further examined the crystal structures of a few as-prepared kinked nanowires using HR-TEM and FFT. The resulting dependence of the number of defects on the length of the nanowires is shown in Figure 5e. The length of the nanowires is approximately proportional to the number of defects. Moreover, the dependence of diffusion coefficients on the number of defects is shown in Figure S9 of the Supporting Information. The data do not fit a simple linear equation, indicating that the diffusion behavior of Cu in these heterodimers is dependent not only on the crystalline defects but also on other factors.[21]

Optical Properties. Cu−Au bimetallic NCs have been previously produced in mostly symmetrical morphologies such as spheres,[78−81] nanorods,[82] and nanocubes.[83] Noble metal NCs with less symmetrical shapes, *e.g.*, branched and kinked nanowires, however, are of great importance in terms of improving localized surface plasmon resonance (LSPR) for surface-enhanced Raman scattering.[84,85] It is well known that noble metals with a fcc crystal lattice tend to crystallize into symmetrical NCs,[86,87] while it remains a challenge to produce branched nanostructures or kinked nanowires for a fcc metal. The outward diffusion of Cu in hetero-oligomers and heterodimers can obviously be

used to produce complex CuAu bimetallic NCs, including nanocage-nanowires and kinked nanowires, respectively. These nanostructures might not be obtainable through direct synthesis. These nanostructures display interesting optical and physical properties. For instance, the hybrid NCs (Figure 4 and Figure 5) produced from hetero-oligomers and heterodimers show a broad LSPR feature from 550 to 1100 nm and 500 to 900 nm, respectively (Figure S10 in the Supporting Information). The NCs with LSPR in the NIR range are appealing for biological applications.[88−91]

CONCLUSION

In conclusion, we demonstrate that preferential Cu outward diffusion during an unconventional galvanic replacement reaction between $HAuCl_4$ and Cu domains within Cu−$Cu_{1.81}S$ hetero-oligomers and Cu−Cu_2S heterodimers leads to the formation of straight and kinked Cu−Au nanowires, respectively. The time-dependent growth of the resulting nanowires provides a method to investigate the kinetic behavior of this metal diffusion process. This study reveals that the nanoscale Cu diffusion behavior can be rationally controlled through the size, the available surface area, and the crystallinity of the starting Cu nanoparticle and the manner of the addition of Au^{3+}. By visualizing the metal diffusion pathway, this method offers a direct measurement of metal interface diffusion in nanomaterial systems. Our current efforts are to extend this protocol to other systems including Ag, Pd, and others.

METHODS

Materials. Copper acetylacetonate ($Cu(acac)_2$, 99.99%), copper chloride ($CuCl_2$, 99.9%), gold chloride trihydrite ($HAuCl_4 \cdot 3H_2O$, 99.9%), 1-dodecanethiol (DDT, 99%), 1-adamantanecarboxylic acid (ACA, 99%), 1,2-hexadecanediol (HDD, 90%), 1-hexadecylamine (HDA, 90%), diphenyl ether (DPE, 99%), and diethylene glycol (DEG, 99%) were purchased from Aldrich. All chemicals and reagents were used as received.

Synthesis. The synthesis of Cu−$Cu_{1.81}S$ hetero-oligomer and Cu−Cu_2S heterodimer hybrid NCs follows our previous reported procedures.[61] The obtained NCs were used for the further diffusion reaction without purification.

Hetero-oligomers and Cu Diffusion. In a typical synthesis of hetero-oligomers, $Cu(acac)_2$ (65 mg, 0.246 mmol), ACA (270 mg, 0.964 mmol), HDD (1.6 g, 6.191 mmol), and HDA (2.0 g, 8.283 mmol) were placed in a 25 mL three-neck flask combined with DPE (10 mL) as a solvent with a condenser in a fume hood. An argon purge system was used during the entire reaction. The solution under vigorous stirring was heated and kept at 100 °C for approximately 1 h. The reaction mixture temperature was then rapidly raised at a rate of 8 °C min^{-1} and kept at 180 °C for about 10−12 h. The resulting solution turned dark purple, indicating the formation of Cu NCs. Then, DDT (0.5 mL, 2.087 mmol) was slowly injected into the remaining solution at 180 °C. The color of the solution slowly turned to blue after 1 h, indicating the formation of Cu−$Cu_{1.81}S$ hetero-oligomers. To obtain the Cu diffusion products, a $HAuCl_4$ solution (95 mg in 3 mL of diethylene glycol) was slowly and dropwise added into the resulting oligomer solution. The color of the solution quickly turned to black after a few minutes. The resulting solution was centrifuged at 14 000 rpm for 5 min, and the supernatant was discarded. The precipitate was redispersed into chloroform and centrifuged again at 14 000 rpm to remove the excess reagent. The manner of the addition of the $HAuCl_4$ solution has a dramatic effect on the resulting NC morphology. The quick and instantaneous addition of the above $HAuCl_4$ solution into the oligomer solution leads to the formation of non-diffusion-controlled products.

Heterodimers and Cu Diffusion. In a typical synthesis of heterodimers, $Cu(acac)_2$ (65 mg, 0.246 mmol), ACA (270 mg, 0.964 mmol), HDD (1.6 g, 6.191 mmol), and HDA (2.0 g, 8.283 mmol) were put in a 25 mL three-neck flask combined with DPE (10 mL) as a solvent with a condenser in a fume hood. A H_2/argon (H_2, 7%) purge system was used during the entire reaction. The solution under vigorous stirring was heated and kept at 100 °C for 2−3 h. The reaction mixture temperature was then rapidly raised at a rate of 8 °C min^{-1} and kept at 180 °C for 2−3 h. During this period, the color of the resulting solution changed from blue to colorless and subsequently to dark purple after 3−4 h. DDT (0.5 mL, 2.087 mmol) was then slowly injected into the remaining solution at 180 °C, and the color of the solution slowly turned to green after 1 h. This observation indicates the formation of Cu−Cu_2S heterodimers. To obtain the Cu diffusion products, a $HAuCl_4$ solution (95 mg in 3 mL of diethylene glycol) was slowly and dropwise added into the resulting dimer solution. The color of the solution quickly turned to black after a few minutes. The resulting solution was centrifuged at 14 000 rpm for 5 min, and the supernatant was discarded. The precipitate was redispersed into chloroform and centrifuged again at 14 000 rpm to remove the excess reagent. Both the addition of 13 mg of $HAuCl_4$ and the quick addition of 95 mg of $HAuCl_4$ into the dimer solution led to the formation of a cage-like morphology for the Cu domain, non-diffusion-controlled products.

Characterization. Samples for transmission electron microscopy characterization were prepared by adding several drops of nanocrystal solutions in chloroform onto 300-mesh copper or nickel grids with carbon support film (no. 01753 or no. 01800, Ted Pella). Samples for scanning electron microscopy (SEM) were prepared by adding a couple drops of nanocrystal solutions in chloroform onto silica wafers. All high-resolution TEM images were taken from JEOL 2100F field-emission and 2100 LaB_6 TEMs at 200 kV, while SEM images were taken on a Hitachi SU-70 Schottky field emission gun scanning electron microscope. Scanning TEM images, energy-dispersive X-ray spectroscopy spectra, and elemental mapping were acquired on a JEOL 2100F field-emission TEM operated at 200 kV. UV−vis absorption spectra were recorded at room temperature with a Shimadzu (BioSpec-1601) UV−vis spectrometer.

Acknowledgment. Y. L. acknowledges the support of a National Research Council (NRC, NIH(NIBIB)/NIST) research associate fellowship. Both authors acknowledge the Maryland NanoCenter and its NispLab (The NispLab is supported in part by the NSF as a MRSEC Shared Experimental Facility). Certain commercial equipment, instruments, or materials are identified in this paper to foster understanding and does not imply recommendation or endorsement by NIST, nor does it imply that the materials or equipment identified are necessarily the best available for the purpose.

Supporting Information Available: EDX analysis of one typical CuAu nanocage and solid CuAu NC produced after the GRR between $HAuCl_4$ and Cu NCs, elemental analysis of branched nanowires, TEM images of the resulting NCs with multiple voids or unevenly distributed metals in Cu domains, TEM images of the solid-core NCs, TEM images of as-prepared NCs with hollow interiors in the Cu domains, elemental analysis of kinked nanowires, TEM images of different kinds of defects observed in kinked nanowires, plot of calculated diffusion coefficients *versus* the number of defects for the kinked nanowires, UV−vis spectra of as-prepared NCs, and TEM images of as-prepared

nanowires showing intact $Cu_{1.81}S$ domains. This material is available free of charge *via* the Internet at http://pubs.acs.org.

REFERENCES AND NOTES

1. Matsukawa, K.; Shirai, K.; Yamaguchi, H.; Katayama-Yoshida, H. Diffusion of Transition-Metal Impurities in Silicon. *Phys. B (Amsterdam, Neth.)* **2007**, *401*, 151–154.
2. Gupta, D. Diffusion in Several Materials Relevant to Cu Interconnection Technology. *Mater. Chem. Phys.* **1995**, *41*, 199–205.
3. Tey, S. H.; Prasad, K.; Tee, K. C.; Chan, L. H.; Seebauer, E. G. Non-Linear Optical Studies of Copper Diffusion at Surfaces and Interfaces of Microelectronic Interconnect Structures. *Thin Solid Films* **2004**, *466*, 217–224.
4. Song, S. X.; Liu, Y. Z.; Li, M.; Mao, D. L.; Chang, C. K.; Ling, H. Q. Diffusion Barrier Performance of W/Ta-W-N Double Layers for Cu Metallization. *Microelectron. Eng.* **2006**, *83*, 423–427.
5. Zhang, X.; Solak, H.; Cerrina, F.; Lai, B.; Cai, Z.; Ilinski, P.; Legnini, D.; Rodrigues, W. X-Ray Microdiffraction Study of Cu Interconnects. *Appl. Phys. Lett.* **2000**, *76*, 315–317.
6. Zhao, C.; Tokei, Z.; Haider, A.; Demuynck, S. Failure Mechanisms of PVD Ta and ALD TaN Barrier Layers for Cu Contact Applications. *Microelectron. Eng.* **2007**, *84*, 2669–2674.
7. Hau-Riege, C. S.; Thompson, C. V. Electromigration in Cu Interconnects with Very Different Grain Structures. *Appl. Phys. Lett.* **2001**, *78*, 3451–3453.
8. Sahoo, K. C.; Chang, C. W.; Wong, Y. Y.; Hsieh, T. L.; Chang, E. Y.; Lee, C. T. Novel Cu/Cr/Ge/Pd Ohmic Contacts on Highly Doped N-GaAs. *J. Electron. Mater.* **2008**, *37*, 901–904.
9. Datye, A. K. Electron Microscopy of Catalysts: Recent Achievements and Future Prospects. *J. Catal.* **2003**, *216*, 144–154.
10. Duffe, S.; Gronhagen, N.; Patryarcha, L.; Sieben, B.; Yin, C. R.; von Issendorff, B.; Moseler, M.; Hovel, H. Penetration of Thin C-60 Films by Metal Nanoparticles. *Nat. Nanotechnol.* **2010**, *5*, 335–339.
11. Mokari, T.; Aharoni, A.; Popov, I.; Banin, U. Diffusion of Gold into InAs Nanocrystals. *Angew. Chem., Int. Ed.* **2006**, *45*, 8001–8005.
12. Yang, J.; Ying, J. Y. Diffusion of Gold from the Inner Core to the Surface of Ag_2S Nanocrystals. *J. Am. Chem. Soc.* **2010**, *132*, 2114–2115.
13. Franchini, I. R.; Bertoni, G.; Falqui, A.; Giannini, C.; Wang, L. W.; Manna, L. Colloidal PbTe-Au Nanocrystal Heterostructures. *J. Mater. Chem.* **2010**, *20*, 1357–1366.
14. Zeng, K. J.; Stierman, R.; Chiu, T. C.; Edwards, D.; Ano, K.; Tu, K. N. Kirkendall Void Formation in Eutectic SnPb Solder Joints on Bare Cu and Its Effect on Joint Reliability. *J. Appl. Phys.* **2005**, *97*, 024508/1–024508/8.
15. Surholt, T.; Herzig, C. Grain Boundary Self-Diffusion in Cu Polycrystals of Different Purity. *Acta Mater.* **1997**, *45*, 3817–3823.
16. Surholt, T.; Mishin, Y. M.; Herzig, C. Grain-Boundary Diffusion and Segregation of Gold in Copper - Investigation in the Type-B and Type-C Kinetic Regimes. *Phys. Rev. B: Condens. Matter* **1994**, *50*, 3577–3587.
17. Elmer, J. W.; Palmer, T. A.; Specht, E. D. Direct Observations of Rapid Diffusion of Cu in Au Thin Films Using in Situ X-Ray Diffraction. *J. Vac. Sci. Technol., A* **2006**, *24*, 978–987.
18. Madakson, P.; Liu, J. C. Interdiffusion and Resistivity of Cu/Au, Cu/Co, Co/Au, and Cu/Co/Au Thin-Films at 25−550 °C. *J. Appl. Phys.* **1990**, *68*, 2121–2126.
19. Gai, P. L.; Smith, B. C.; Owen, G. Bulk Diffusion of Metal Particles on Ceramic Substrates. *Nature* **1990**, *348*, 430–432.
20. Horch, S.; Lorensen, H. T.; Helveg, S.; Laegsgaard, E.; Stensgaard, I.; Jacobsen, K. W.; Norskov, J. K.; Besenbacher, F. Enhancement of Surface Self-Diffusion of Platinum Atoms by Adsorbed Hydrogen. *Nature* **1999**, *398*, 134–136.
21. Feibelman, P. J. Formation and Diffusion of S-Decorated Cu Clusters on Cu(111). *Phys. Rev. Lett.* **2000**, *85*, 606–609.
22. Wang, K. D.; Zhang, C.; Loy, M. M. T.; Xiao, X. D. Time-Dependent Tunneling Spectroscopy for Studying Surface Diffusion Confined in Nanostructures. *Phys. Rev. Lett.* **2005**, *94*, 036103/1–036103/4.
23. Cui, Y.; Bjork, M. T.; Liddle, J. A.; Sonnichsen, C.; Boussert, B.; Alivisatos, A. P. Integration of Colloidal Nanocrystals into Lithographically Patterned Devices. *Nano Lett.* **2004**, *4*, 1093–1098.
24. Chen, J. Y.; Mela, P.; Moller, M.; Lensen, M. C. Microcontact Deprinting: A Technique to Pattern Gold Nanoparticles. *ACS Nano* **2009**, *3*, 1451–1456.
25. Wolfrum, B.; Mourzina, Y.; Mayer, D.; Schwaab, D.; Offenhausser, A. Fabrication of Large-Scale Patterned Gold-Nanopillar Arrays on a Silicon Substrate Using Imprinted Porous Alumina Templates. *Small* **2006**, *2*, 1256–1260.
26. Henzie, J.; Barton, J. E.; Stender, C. L.; Odom, T. W. Large-Area Nanoscale Patterning: Chemistry Meets Fabrication. *Acc. Chem. Res.* **2006**, *39*, 249–257.
27. Homberger, M.; Simon, U. On the Application Potential of Gold Nanoparticles in Nanoelectronics and Biomedicine. *Phil. Trans. R. Soc. A* **2010**, *368*, 1405–1453.
28. Xiong, X.; Busnaina, A.; Selvarasah, S.; Somu, S.; Wei, M.; Mead, J.; Chen, C. L.; Aceros, J.; Makaram, P.; Dokmeci, M. R. Directed Assembly of Gold Nanoparticle Nanowires and Networks for Nanodevices. *Appl. Phys. Lett.* **2007**, *91*, 063101/1–063101/3.
29. Koh, S. J. Controlled Placement of Nanoscale Building Blocks: Toward Large-Scale Fabrication of Nanoscale Devices. *JOM* **2007**, *59*, 22–28.
30. Jeon, H. S.; Cho, C. W.; Lim, C. H.; Park, B.; Ju, H.; Kim, S.; Lee, S. B. Nanoscale Floating-Gate Characteristics of Colloidal Au Nanoparticles Electrostatically Assembled on Si Nanowires. *J. Vac. Sci. Technol., B* **2006**, *24*, 3192–3195.
31. Barry, C. R.; Jacobs, H. O. Fringing Field Directed Assembly of Nanomaterials. *Nano Lett.* **2006**, *6*, 2790–2796.
32. Huang, J. X.; Tao, A. R.; Connor, S.; He, R. R.; Yang, P. D. A General Method for Assembling Single Colloidal Particle Lines. *Nano Lett.* **2006**, *6*, 524–529.
33. Foster, E. W.; Kearns, G. J.; Goto, S.; Hutchison, J. E. Patterned Gold-Nanoparticle Monolayers Assembled on the Oxide of Silicon. *Adv. Mater.* **2005**, *17*, 1542–1545.
34. Gates, B. D.; Xu, Q. B.; Stewart, M.; Ryan, D.; Willson, C. G.; Whitesides, G. M. New Approaches to Nanofabrication: Molding, Printing, and Other Techniques. *Chem. Rev.* **2005**, *105*, 1171–1196.
35. Ling, X.; Zhu, X.; Zhang, J.; Zhu, T.; Liu, M. H.; Tong, L. M.; Liu, Z. F. Reproducible Patterning of Single Au Nanoparticles on Silicon Substrates by Scanning Probe Oxidation and Self-Assembly. *J. Phys. Chem. B* **2005**, *109*, 2657–2665.
36. Shevchenko, E. V.; Ringler, M.; Schwemer, A.; Talapin, D. V.; Klar, T. A.; Rogach, A. L.; Feldmann, J.; Alivisatos, A. P. Self-Assembled Binary Superlattices of CdSe and Au Nanocrystals and Their Fluorescence Properties. *J. Am. Chem. Soc.* **2008**, *130*, 3274–3275.
37. Shevchenko, E. V.; Talapin, D. V.; Kotov, N. A.; O'Brien, S.; Murray, C. B. Structural Diversity in Binary Nanoparticle Superlattices. *Nature* **2006**, *439*, 55–59.
38. Chen, W.; Yu, R.; Li, L. L.; Wang, A. N.; Peng, Q.; Li, Y. D. A Seed-Based Diffusion Route to Monodisperse Intermetallic CuAu Nanocrystals. *Angew. Chem., Int. Ed.* **2010**, *49*, 2917–2921.
39. Au, L.; Lu, X. M.; Xia, Y. N. A Comparative Study of Galvanic Replacement Reactions Involving Ag Nanocubes and $AuCl_2^-$ or $AuCl_4^-$. *Adv. Mater.* **2008**, *20*, 2517–2522.
40. Guo, S. J.; Dong, S. J.; Wang, E. A General Method for the Rapid Synthesis of Hollow Metallic or Bimetallic Nanoelectrocatalysts with Urchinlike Morphology. *Chem.—Eur. J.* **2008**, *14*, 4689–4695.
41. Fang, J. X.; Ma, X. N.; Cai, H. H.; Song, X. P.; Ding, B. J. Nanoparticle-Aggregated 3d Monocrystalline Gold Dendritic Nanostructures. *Nanotechnology* **2006**, *17*, 5841–5845.
42. Zhang, Q. B.; Xie, J. P.; Liang, J.; Lee, J. Y. Synthesis of Monodisperse Ag-Au Alloy Nanoparticles with Independently Tunable Morphology, Composition, Size, and

Surface Chemistry and Their 3-D Superlattices. *Adv. Funct. Mater.* **2009**, *19*, 1387–1398.
43. Kim, M. H.; Lu, X. M.; Wiley, B.; Lee, E. P.; Xia, Y. N. Morphological Evolution of Single-Crystal Ag Nanospheres during the Galvanic Replacement Reaction with $HAuCl_4$. *J. Phys. Chem. C* **2008**, *112*, 7872–7876.
44. Wang, Y. L.; Cai, L.; Xia, Y. N. Monodisperse Spherical Colloids of Pb and Their Use as Chemical Templates to Produce Hollow Particles. *Adv. Mater.* **2005**, *17*, 473–477.
45. Lu, X. M.; Tuan, H. Y.; Chen, J. Y.; Li, Z. Y.; Korgel, B. A.; Xia, Y. N. Mechanistic Studies on the Galvanic Replacement Reaction between Multiply Twinned Particles of Ag and $HAuCl_4$ in an Organic Medium. *J. Am. Chem. Soc.* **2007**, *129*, 1733–1742.
46. Aherne, D.; Gara, M.; Kelly, J. M.; Gun'ko, Y. K. From Ag Nanoprisms to Triangular AuAg Nanoboxes. *Adv. Funct. Mater.* **2010**, *20*, 1329–1338.
47. Lu, X.; Au, L.; McLellan, J.; Li, Z.-Y.; Marquez, M.; Xia, Y. Fabrication of Cubic Nanocages and Nanoframes by Dealloying Au/Ag Alloy Nanoboxes with an Aqueous Etchant Based on $Fe(NO_3)_3$ or NH_4OH. *Nano Lett.* **2007**, *7*, 1764–1769.
48. Skrabalak, S. E.; Au, L.; Li, X. D.; Xia, Y. Facile Synthesis of Ag Nanocubes and Au Nanocages. *Nat. Protoc.* **2007**, *2*, 2182–2190.
49. Jose-Yacaman, M.; Gutierrez-Wing, C.; Miki, M.; Yang, D. Q.; Piyakis, K. N.; Sacher, E. Surface Diffusion and Coalescence of Mobile Metal Nanoparticles. *J. Phys. Chem. B* **2005**, *109*, 9703–9711.
50. Gautam, A. R. S.; Howe, J. M. In Situ TEM Study of Au-Cu Alloy Nanoparticle Migration and Coalescence. *J. Mater. Sci.* **2009**, *44*, 601–607.
51. Zheng, H. M.; Claridge, S. A.; Minor, A. M.; Alivisatos, A. P.; Dahmen, U. Nanocrystal Diffusion in a Liquid Thin Film Observed by in Situ Transmission Electron Microscopy. *Nano Lett.* **2009**, *9*, 2460–2465.
52. Roder, H.; Hahn, E.; Brune, H.; Bucher, J. P.; Kern, K. Building One-Dimensional and 2-Dimensional Nanostructures by Diffusion-Controlled Aggregation at Surfaces. *Nature* **1993**, *366*, 141–143.
53. Horvath, J.; Birringer, R.; Gleiter, H. Diffusion in Nanocrystalline Material. *Solid State Commun.* **1987**, *62*, 319–322.
54. Smigelskas, A. D.; Kirkendall, E. O. Zinc Diffusion in Alpha-Brass. *Trans. Am. Inst. Min. Metall. Eng.* **1947**, *171*, 130–142.
55. Sun, Y.; Mayers, B. T.; Xia, Y. Template-Engaged Replacement Reaction: A One-Step Approach to the Large-Scale Synthesis of Metal Nanostructures with Hollow Interiors. *Nano Lett.* **2002**, *2*, 481–485.
56. Sun, Y.; Wiley, B.; Li, Z.-Y.; Xia, Y. Synthesis and Optical Properties of Nanorattles and Multiple-Walled Nanoshells/Nanotubes Made of Metal Alloys. *J. Am. Chem. Soc.* **2004**, *126*, 9399–9406.
57. Sun, Y.; Xia, Y. Increased Sensitivity of Surface Plasmon Resonance of Gold Nanoshells Compared to That of Gold Solid Colloids in Response to Environmental Changes. *Anal. Chem.* **2002**, *74*, 5297–5305.
58. Sun, Y.; Xia, Y. Alloying and Dealloying Processes Involved in the Preparation of Metal Nanoshells through a Galvanic Replacement Reaction. *Nano Lett.* **2003**, *3*, 1569–1572.
59. Sun, Y.; Xia, Y. Multiple-Walled Nanotubes Made of Metals. *Adv. Mater.* **2004**, *16*, 264–268.
60. Cabot, A.; Smith, R. K.; Yin, Y. D.; Zheng, H. M.; Reinhard, B. M.; Liu, H. T.; Alivisatos, A. P. Sulfidation of Cadmium at the Nanoscale. *ACS Nano* **2008**, *2*, 1452–1458.
61. Liu, Y.; Walker, A. R. H. Facile One-Pot Synthesis of Metal-Semiconductor Hybrid Nanocrystals Via Chemical Transformation: The Case of Cu-Cu_xS Heterodimers and Hetero-Oligomers. *J. Phys. Chem. C* **2010**, *114*, 4264–4271.
62. Xu, C. X.; Zhang, Y.; Wang, L. Q.; Xu, L. Q.; Bian, X. F.; Ma, H. Y.; Ding, Y. Nanotubular Mesoporous PdCu Bimetallic Electrocatalysts toward Oxygen Reduction Reaction. *Chem. Mater.* **2009**, *21*, 3110–3116.
63. O'Mullane, A. P.; Ippolito, S. J.; Bond, A. M.; Bhargava, S. K. A Study of Localised Galvanic Replacement of Copper and Silver Films with Gold Using Scanning Electrochemical Microscopy. *Electrochem. Commun.* **2010**, *12*, 611–615.
64. Railsback, J. G.; Johnston-Peck, A. C.; Wang, J. W.; Tracy, J. B. Size-Dependent Nanoscale Kirkendall Effect During the Oxidation of Nickel Nanoparticles. *ACS Nano* **2010**, *4*, 1913–1920.
65. Sun, Y.; Mayers, B.; Xia, Y. Metal Nanostructures with Hollow Interiors. *Adv. Mater.* **2003**, *15*, 641–646.
66. Fan, H. J.; Gosele, U.; Zacharias, M. Formation of Nanotubes and Hollow Nanoparticles Based on Kirkendall and Diffusion Processes: A Review. *Small* **2007**, *3*, 1660–1671.
67. Teng, X. W.; Wang, Q.; Liu, P.; Han, W.; Frenkel, A.; Wen, W.; Marinkovic, N.; Hanson, J. C.; Rodriguez, J. A. Formation of Pd/Au Nanostructures from Pd Nanowires Via Galvanic Replacement Reaction. *J. Am. Chem. Soc.* **2008**, *130*, 1093–1101.
68. Wang, Z. L. Transmission Electron Microscopy of Shape-Controlled Nanocrystals and Their Assemblies. *J. Phys. Chem. B* **2000**, *104*, 1153–1175.
69. Xia, Y. N.; Xiong, Y. J.; Lim, B.; Skrabalak, S. E. Shape-Controlled Synthesis of Metal Nanocrystals: Simple Chemistry Meets Complex Physics? *Angew. Chem., Int. Ed.* **2009**, *48*, 60–103.
70. Dovgolevsky, E.; Haick, H. Direct Observation of the Transition Point between Quasi-Spherical and Cubic Nanoparticles in Two-Step Seed-Mediated Growth Method. *Small* **2008**, *4*, 2059–2066.
71. Mori, H.; Komatsu, M.; Takeda, K.; Fujita, H. Spontaneous Alloying of Copper into Gold Atom Clusters. *Philos. Mag. Lett.* **1991**, *63*, 173–178.
72. Zhang, Q.; Lee, J. Y.; Yang, J.; Boothroyd, C.; Zhang, J. Size and Composition Tunable Ag-Au Alloy Nanoparticles by Replacement Reactions. *Nanotechnology* **2007**, *18*, 245605/1–245605/8.
73. Yasuda, H.; Mori, H.; Komatsu, M.; Takeda, K. Spontaneous Alloying of Copper Atoms into Gold Clusters at Reduced Temperatures. *J. Appl. Phys.* **1993**, *73*, 1100–1103.
74. Yasuda, H.; Mori, H.; Komatsu, M.; Takeda, K.; Fujita, H. In Situ Observation of Spontaneous Alloying in Atom Clusters. *J. Electron Microsc.* **1992**, *41*, 267–269.
75. Lu, X. M.; Chen, J. Y.; Skrabalak, S. E.; Xia, Y. N. Galvanic Replacement Reactions: A Simple and Powerful Route to Hollow and Porous Metal Nanostructures. *Proc. Inst. Mech. Eng. N: J. Nanoeng. Nanosyst.* **2008**, *221*, 1–16.
76. Wang, C.; Wei, Y. J.; Jiang, H. Y.; Sun, S. H. Bending Nanowire Growth in Solution by Mechanical Disturbance. *Nano Lett.* **2010**, *10*, 2121–2125.
77. Hartung, F.; Ewert, J. C.; Dzick, J.; Schmitz, G. Interreaction of Cu/Au Thin Films Observed by High Angle Hollow Cone Darkfield Electron Microscopy. *Scr. Mater.* **1998**, *39*, 79–85.
78. Chen, W.; Yu, R.; Li, L. L.; Wang, A. N.; Peng, Q.; Li, Y. D. A Seed-Based Diffusion Route to Monodisperse Intermetallic CuAu Nanocrystals. *Angew. Chem., Int. Ed.* **2010**, *49*, 2917–2921.
79. Sra, A. K.; Ewers, T. D.; Schaak, R. E. Direct Solution Synthesis of Intermetallic AuCu and $AuCu_3$ Nanocrystals and Nanowire Networks. *Chem. Mater.* **2005**, *17*, 758–766.
80. Sra, A. K.; Schaak, R. E. Synthesis of Atomically Ordered AuCu and $AuCu_3$ Nanocrystals from Bimetallic Nanoparticle Precursors. *J. Am. Chem. Soc.* **2004**, *126*, 6667–6672.
81. Schaak, R. E.; Sra, A. K.; Leonard, B. M.; Cable, R. E.; Bauer, J. C.; Han, Y. F.; Means, J.; Teizer, W.; Vasquez, Y.; Funck, E. S. Metallurgy in a Beaker: Nanoparticle Toolkit for the Rapid Low-Temperature Solution Synthesis of Functional Multimetallic Solid-State Materials. *J. Am. Chem. Soc.* **2005**, *127*, 3506–3515.
82. Henkel, A.; Jakab, A.; Brunklaus, G.; Sonnichsen, C. Tuning Plasmonic Properties by Alloying Copper into Gold Nanorods. *J. Phys. Chem. C* **2009**, *113*, 2200–2204.
83. Liu, Y.; Walker, A. H. Monodisperse Gold−Copper Bimetallic Nanocubes: Facile One-Step Synthesis with Controllable Size and Composition. *Angew. Chem., Int. Ed.* **2010**, *49*, 6781–6785.
84. Hao, E.; Bailey, R. C.; Schatz, G. C.; Hupp, J. T.; Li, S. Y. Synthesis and Optical Properties of "Branched" Gold Nanocrystals. *Nano Lett.* **2004**, *4*, 327–330.

85. Bakr, O. M.; Wunsch, B. H.; Stellacci, F. High-Yield Synthesis of Multi-Branched Urchin-Like Gold Nanoparticles. *Chem. Mater.* **2006**, *18*, 3297–3301.
86. Sanchez-Iglesias, A.; Grzelczak, M.; Rodriguez-Gonzalez, B.; Alvarez-Puebla, R. A.; Liz-Marzan, L. M.; Kotov, N. A. Gold Colloids with Unconventional Angled Shapes. *Langmuir* **2009**, *25*, 11431–11435.
87. Li, Z. Q.; Li, W. Y.; Camargo, P. H. C.; Xia, Y. N. Facile Synthesis of Branched Au Nanostructures by Templating against a Self-Destructive Lattice of Magnetic Fe Nanoparticles. *Angew. Chem., Int. Ed.* **2008**, *47*, 9653–9656.
88. Skrabalak, S. E.; Au, L.; Lu, X. M.; Li, X. D.; Xia, Y. N. Gold Nanocages for Cancer Detection and Treatment. *Nanomedicine* **2007**, *2*, 657–668.
89. Skrabalak, S. E.; Chen, J. Y.; Sun, Y. G.; Lu, X. M.; Au, L.; Cobley, C. M.; Xia, Y. N. Gold Nanocages: Synthesis, Properties, and Applications. *Acc. Chem. Res.* **2008**, *41*, 1587–1595.
90. Yang, X. M.; Skrabalak, S. E.; Li, Z. Y.; Xia, Y. N.; Wang, L. H. V. Photoacoustic Tomography of a Rat Cerebral Cortex in Vivo with Au Nanocages as an Optical Contrast Agent. *Nano Lett.* **2007**, *7*, 3798–3802.
91. Chen, J. Y.; Wang, D. L.; Xi, J. F.; Au, L.; Siekkinen, A.; Warsen, A.; Li, Z. Y.; Zhang, H.; Xia, Y. N.; Li, X. D. Immuno Gold Nanocages with Tailored Optical Properties for Targeted Photothermal Destruction of Cancer Cells. *Nano Lett.* **2007**, *7*, 1318–1322.